Mon. Not. R. Astron. Soc. **276**, 167–181 (1995)

Photoionization modelling based on *HST* images of Magellanic Cloud planetary nebulae – I. SMC N 2 and SMC N 5

X.-W. Liu,[1] M. J. Barlow,[1] J. C. Blades,[2] S. Osmer[2] and R. E. S. Clegg[3]
[1] *Department of Physics and Astronomy, University College London, Gower Street, London WC1E 6BT*
[2] *Space Telescope Science Institute, 3700 San Martin Drive, Baltimore, MD 21218, USA*
[3] *Royal Greenwich Observatory, Madingley Road, Cambridge CB3 0EX*

Accepted 1995 March 17. Received 1995 March 17; in original form 1994 December 16

ABSTRACT

We construct fully self-consistent, detailed photoionization models for two planetary nebulae (PNe) in the Small Magellanic Cloud (SMC), namely SMC N 2 and SMC N 5, to fit optical and UV spectrophotometric observations as well as *HST* Faint Object Camera (FOC) narrow-band images taken in the light of Hβ. The derived density structure shows that both PNe have a central cavity surrounded by a shell of decreasing density described by a parabolic curve. For both nebulae, our models fail to reproduce the *HST* images taken in the light of the [O III] λ5007 line, in the sense that the observed [O III] λ5007 surface brightness decreases more slowly outside the peak emission than predicted. An effective temperature of $T_{\rm eff}$ = 111 500 K, a stellar surface gravity of log g = 5.45 and a luminosity of L_* = 8430 $L_\odot$ are derived for the central star of SMC N2; similarly $T_{\rm eff}$ = 137 500 K, log g = 6.0 and L_* = 5850 $L_\odot$ are derived for SMC N 5. SMC N 2 is optically thin and has a total nebular mass (H plus He) of 0.180 $M_\odot$, while SMC N 5 is optically thick and has an ionized gas mass of 0.194 $M_\odot$. Using the H-burning SMC metal abundance (Z = 0.004) evolutionary tracks calculated by Vassiliadis & Wood, core masses of 0.674 $M_\odot$ and 0.649 $M_\odot$ are derived for SMC N 2 and SMC N 5, respectively. Similarly, from the He-burning evolutionary tracks of Vassiliadis & Wood for progenitor stars of mean LMC heavy-element abundance (Z = 0.008), we find M_c = 0.695 and 0.675 $M_\odot$ for SMC N 2 and SMC N 5, respectively. We find that Hβ images are needed if one is to derive accurate stellar luminosities directly from photoionization modelling. However, in the absence of an Hβ image, photoionization models based on [O III] images (and nebular line intensities) yield accurate values of $T_{\rm eff}$ and log g, which in turn allow reliable stellar masses and luminosities to be derived from a comparison with theoretical evolutionary tracks. We show that the correct nebular ionized mass can be deduced from the nebular Hβ flux, provided the mean nebular density given by the C III] λ1909/λ1907 ratio is also known.

Key words: ISM: abundances – planetary nebulae: individual: SMC N2 – planetary nebulae: individual: SMC N5 – Magellanic Clouds.

1 INTRODUCTION

With the advent of the unprecedented spatial resolution provided by *Hubble Space Telescope* (*HST*) imaging, it is now possible to make detailed, fully self-consistent studies of individual planetary nebulae (PNe) in the Magellanic Clouds. These PNe are good objects to study because their distances are well established. In contrast, distances to individual Galactic PNe are usually uncertain by at least 50 per cent (see Gathier et al. 1983). Accurate distances are essential for deriving fundamental parameters such as the luminosity of an exciting star and its core mass, and thus for establishing its evolutionary status. Accurate distances are also required in order to determine the masses of the gaseous shells, which are needed to address questions such as the chemical enrichment of the interstellar medium by low-to-intermediate-mass stars, as well as the mass-loss history of the progenitor asymptotic giant branch (AGB) stars. When compared to

PNe in the Galactic Bulge, the Magellanic Cloud PNe have the additional advantage of a very low interstellar extinction, which enables them to be easily accessible in the UV wavelength band which is vital for the study of key elements such as carbon.

Given the advantages and potential of Magellanic Cloud PNe in understanding post-AGB evolution, in the past 10 years a significant number of studies on this topic have been published; for recent reviews see Barlow (1989) and Dopita (1993). Magellanic Cloud PNe are, however, much smaller in angular diameter than Galactic PNe, mostly less than 2 arcsec and often less than 1 arcsec, and thus cannot be resolved easily from the ground at the present time, except for about half a dozen relatively old and faint PNe (Jacoby 1980). Special technique such as speckle interferometry has been employed to derive the nebular surface brightness and density distribution for a handful of bright PNe (Barlow et al. 1986; Wood, Bessell & Dopita 1986). Wood et al. (1987) used a ground-based direct imaging technique to determine the angular diameters of fainter, larger Magellanic Cloud PNe. These studies provided important information, but details of the morphology of the nebulae remained unknown. Unfortunately, the density distribution derived from speckle interferometry depends on the geometric structures assumed, and a detailed knowledge of the density distribution is required to derive reliable nebular masses and to construct self-consistent photoionization models. The latter are crucial for evaluating the effect of nebular optical depth, in order that an accurate luminosity for the exciting star can be determined.

HST Faint Object Camera (FOC) images have recently been presented by Blades et al. (1992, 1995 in preparation) for a large sample of Magellanic Cloud PNe, in the light of [O III] λ5007 and in Hβ for a few of them. These include several secured after the 1993 December servicing mission which corrected the aberrated optics of the *HST*. Dopita et al. (1993, 1994) have presented *HST* Wide Field Planetary Camera imaging for two LMC PNe, LMC N 66 in the light of Hα + [N II] λ6584 and [O III] λ5007, and LMC SMP 85 in the light of [O III] λ5007, as well as photoionization modelling calculations based on these images. In both cases, in order to fit the very complex ionization structure and/or morphology, these authors were forced to adopt a two-component model, in which one component was optically thin while the other was optically thick or had a much higher density. A similar two-component model was used by Clegg et al. (1987) to model the Galactic PN NGC 3918. Although it may be physically more realistic for these particular cases, two component modelling calculations cannot be treated rigorously by the currently available photoionization modelling codes, and are therefore ad hoc in some sense. For example, in such cases it is no longer possible to treat the ionization and thermal structures fully self-consistently, not to mention the somewhat arbitrary weighting of contributions from the two components and the sacrifice in accuracy in the treatment of the diffuse ionizing radiation field.

We have begun the photoionization modelling of objects in the Blades et al. (1992, 1995 in preparation) survey. In this paper, we present detailed, fully self-consistent photoionization models for two SMC PNe, namely SMC N 2 (SMP 2) and SMC N 5 (SMP 5). In addition to optical and UV spectrophotometric data published previously, *HST* FOC monochromatic images in the light of Hβ are used to construct realistic density distributions. These two nebulae were selected because both of them possess a high degree of azimuthal symmetry and are well resolved by the *HST*. In addition, they are two out of only four Magellanic Cloud PNe that have so far been imaged in the light of Hβ by the *HST* (the other two are LMC N 201 and LMC N 66). In addition to the information on SMC N 2 and SMC N 5, the modelling calculations presented here may provide a direct check on the capabilities and limitations of current modelling procedures and photoionization codes. In Section 2, we describe the observational data and the ingredients used to construct the models, which are presented and compared to the observations in Section 3. The nebular and stellar masses derived from our models are presented in Section 4.

2 OBSERVATIONAL DATA

2.1 Nebular surface brightness distributions

The Hβ and [O III] λ5007 images of SMC N 2 and SMC N 5 analysed here were secured by Blades et al. (1992) using the *HST* FOC in 1991 July 9, before the implementation of the COSTAR corrective optics. The detector was a photon-counting system, and each pixel projected to 0.0224 arcsec on the sky. The images were flat-fielded, réseau marks were removed, and the images were then deconvolved using 50 iterations of the Richardson–Lucy method (Richardson 1972; Lucy 1974). As described by Blades et al. (1995, in preparation), comparison between images secured after the implementation of COSTAR with those observed before and then deconvolved using the Richardson–Lucy method, shows that this image restoration algorithm works extremely well and is capable of recovering details to a high degree of accuracy. The Hβ and [O III] λ5007 narrow-band filters have effective wavelengths of 4870 and 5010 Å and effective bandwidths of 36.7 and 35.5 Å, respectively. For both nebulae, the contribution from nebular continuum emission to the Hβ images is estimated to be about 3 per cent, and to be less than 0.5 per cent for the λ5007 images, and is therefore neglected in the analysis. For both objects, no exciting central stars were detected on the images taken through either filter. The deconvolved Hβ images are presented in Fig. 1. The [O III] λ5007 images have been previously published by Blades et al. (1992), but for convenience they are also reproduced in Fig. 1.

The azimuthally averaged surface brightness distributions in the Hβ and λ5007 lines were derived using an algorithm implemented in the SURFPHOT package of MIDAS.[1] Since no central stars are detected and both nebulae possess a high degree of azimuthal symmetry, we have defined the gravity centres of the surface brightness as the nebular centres. The integrated flux within a radius r as a function of r was then calculated. For a given radius r, the contribution from pixels for which only part falls inside the circle of radius r was calculated using a differential method. To minimize the error, each pixel of the original images was rebinned to 5 × 5 pixels. Finally, the integrated flux within radius r as a function of r was differentiated with respect to r and then divided by $2\pi r$

[1] MIDAS is developed and distributed by the European Southern Observatory.

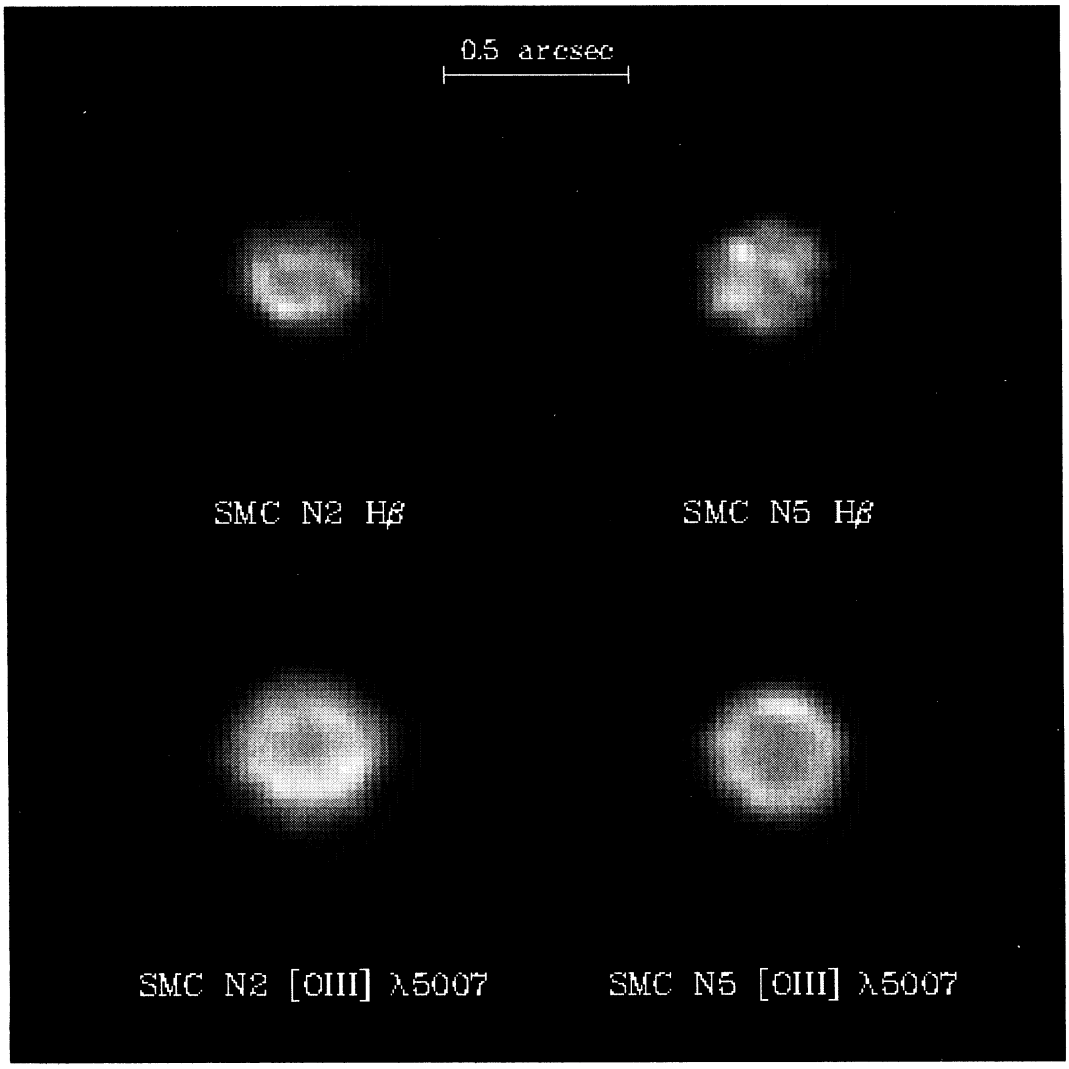

Figure 1. *HST* FOC images of SMC N 2 and SMC N 5 in the light of Hβ and [O III] λ5007. The images have been deconvolved by 50 iterations of the Richardson–Lucy method. Each pixel projects to 0.0224 arcsec on the sky.

to obtain the required azimuthally averaged surface brightness distributions. The results are plotted in Fig. 2.

2.2 Optical and UV spectrophotometry

Optical spectrophotometric measurements of SMC N 2 and SMC N 5 have been presented by Aller et al. (1981), Barlow (1987), Monk, Barlow & Clegg (1988) and Meatheringham & Dopita (1991). The line intensities adopted here are based on the first two references. These two nebulae were observed by *IUE* using the large aperture in 1981 and 1983. These *IUE* observations, together with optical spectrophotometric data, have been analysed by Aller et al. (1987) and by Walton, Barlow & Clegg (1991 and in preparation). The UV dereddened relative intensities listed in Table 1 were taken from Walton et al. (in preparation).

The absolute Hβ fluxes of SMC N 2 and SMC N 5 were measured by Osmer (1976), Webster (1983), Wood et al. (1987) and Meatheringham et al. (1988). We adopt log $F(\mathrm{H}\beta) = -12.76$ and -12.81 cgs for SMC N 2 and SMC N 5, respectively. These values are probably accurate to 0.02 dex.

Both SMC N 2 and SMC N 5 are of relatively high excitation class, and the He II λ1640 line is clearly detected by *IUE*. The total interstellar reddening toward the objects, including contributions from our own Galaxy and the host galaxy, were derived by comparing the observed He II $I(\lambda1640)/I(\lambda4686)$ ratios to their case B theoretical values (Hummer & Storey 1987). The Galactic reddening law of Howarth (1983) and the SMC reddening law of Prévot et al. (1984) were used. The contribution from Galactic reddening was derived from the reddening map of Burstein & Heiles (1982), and the observed $I(\lambda1640)/I(\lambda4686)$ ratio was used to derive the remaining SMC reddening. We found $c(\mathrm{Gal}) = 0.065$ and $c(\mathrm{SMC}) = 0.015$ for SMC N 2, where c is the logarithmic extinction at Hβ. Similarly, $c(\mathrm{Gal}) = 0.065$ and $c(\mathrm{SMC}) = 0.097$ were derived for SMC N 5. The observed line intensities listed in Table 1 have been corrected for interstellar reddening and are normalized so that $I(\mathrm{H}\beta) = 100$. The Hβ surface brightness distributions of SMC N 2 and SMC N 5, deduced from the *HST* images shown in Fig. 2, are normalized so that the total dereddened fluxes are respectively log $I(\mathrm{H}\beta) = -12.68$ and -12.65 (erg cm^{-2} s^{-1}). The

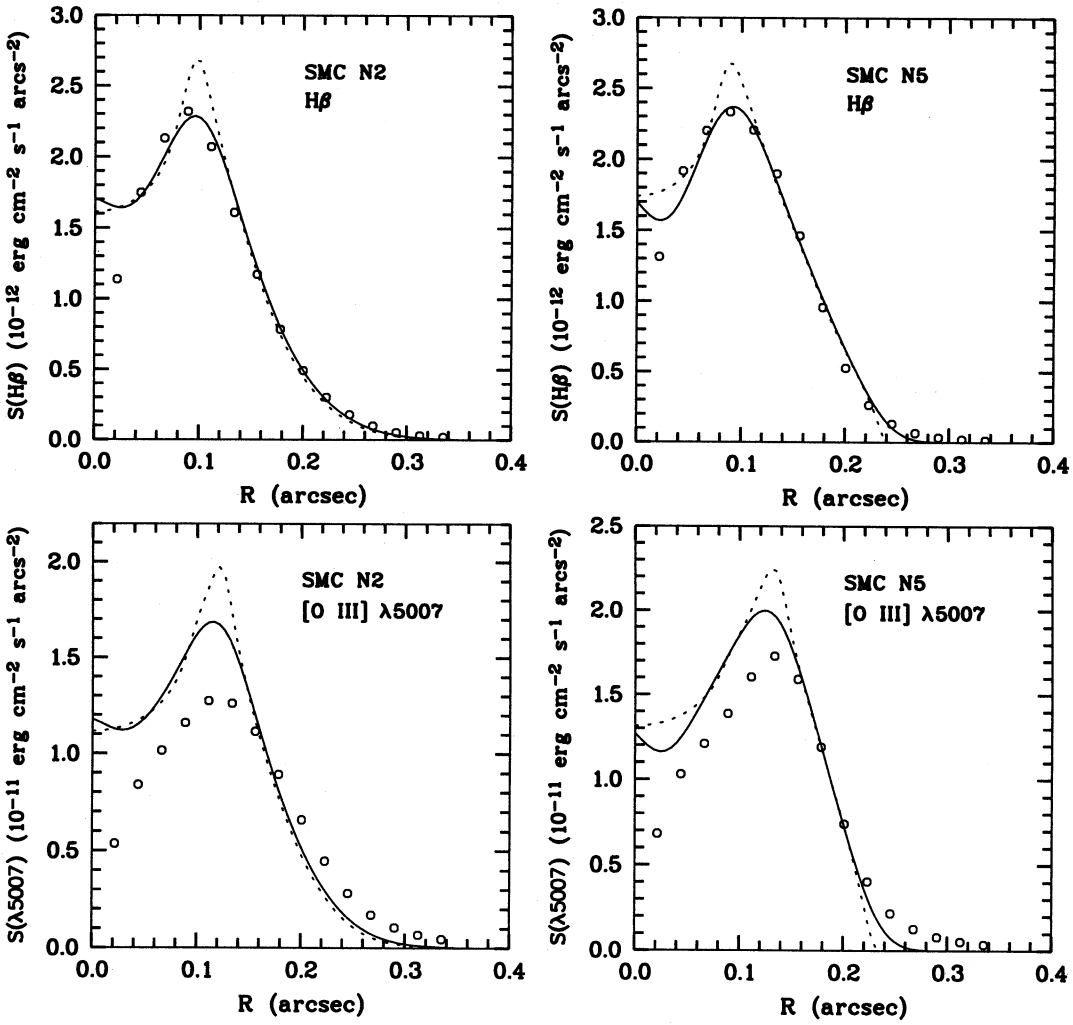

Figure 2. Azimuthally averaged surface brightness distributions in the light of Hβ and [O III] λ5007 for SMC N 2 and SMC N 5 derived from the *HST* FOC images (open circles). The dotted and solid lines are, respectively, the intrinsic surface brightness distributions predicted by the models, and the same distributions after convolution with a Gaussian of FWHM of 0.05 arcsec.

[O III] λ5007 surface brightness distributions are then normalized using the intensities of $I(\lambda4959+\lambda5007)$ relative to Hβ as listed in Table 1, assuming $I(\lambda5007)=2.88I(\lambda4959)$ (Nussbaumer & Storey 1981).

Recently, in a programme aimed at studying the ^{13}C to ^{12}C isotope ratios in PNe, Clegg, Storey & Walsh (private communication) have measured the C III] $I(\lambda1909)/I(\lambda1907)$ ratio in SMC N 2 using the *HST* Goddard High Resolution Spectrograph. This line ratio is a sensitive density diagnostic, and is particularly useful for detecting regimes of higher densities ($\geq 10^4$ cm^{-3}), where classical density diagnostic ratios such as [O II] $I(\lambda3729)/I(\lambda3726)$ and [S II] $I(\lambda6716)/I(\lambda6731)$ approach their high density limits (Nussbaumer & Schild 1979). They find $I(\lambda1909)/I(\lambda1907)=0.794$, which gives $N_e=7980$ cm^{-3} for a temperature of 13 450 K, using the atomic data of Keenan, Feibelman & Berrington (1992). This density is about a factor of 3 higher than that deduced from the [O II] $I(\lambda3729)/I(\lambda3726)$ ratio, $N_e=3080$ cm^{-3}. As we will see in the next section, the radial density distribution derived for SMC N 2 from its Hβ image reproduces naturally these two density sensitive ratios.

Finally, we adopt a distance modulus of 18.9 to the SMC, corresponding to a distance of 60.3 kpc. This distance to the SMC is slightly larger than the 57.5 kpc used by Barlow et al. (1986).

3 PHOTOIONIZATION MODELS

3.1 Density distribution

Under typical nebular conditions, the mean free path of a hydrogen ionizing photon is much smaller than the characteristic size of the nebula. A nebula can either be optically thin, where all the H atoms are ionized to H^+ (density-bounded), or be optically thick, where only part of it is ionized (radiation-bounded). In the latter case the nebula is composed of two distinct zones, i.e. a central region where the hydrogen is nearly fully ionized (Strömgren sphere) and a neutral envelope separated from the ionized zone by a thin transition region. Unlike the [O III] λ5007 line, which is collisionally excited and has an emissivity which depends strongly on the electron temperature and density, Hβ origin-

Table 1. Photoionization model of SMC N 2 and SMC N 5.

Model setup	SMC N 2	SMC N 5
$T_{\rm eff}$ (K):	111500	137500
$\log g$:	5.45	6.00
L_* ($L_\odot$):	8430	5850
ε:	0.405	0.700
Density distribution:	Fig. 3(a), solid curve	Fig. 3(b), solid curve
Nebular abundances relative to H (by number):		
He:	9.77×10^{-2}	1.13×10^{-1}
C:	5.17×10^{-4}	9.75×10^{-4}
N:	1.77×10^{-5}	2.15×10^{-5}
O:	1.43×10^{-4}	2.05×10^{-4}
Ne:	2.19×10^{-5}	3.11×10^{-5}
S:	3.70×10^{-6}	3.17×10^{-6}

Comparison between observations and model predictions:

	SMC N 2		SMC N 5	
Properties	Observed	Model	Observed	Model
$\log I(\mathrm{H}\beta)$ (ergs cm^{-2} sec^{-1})	-12.68	-12.68	-12.65	-12.65
He IIλ4686/He Iλ5876	2.58	2.57	3.92	3.91
C IV(λ1548 + λ1550)/C III](λ1907 + λ1909)	1.09	1.41	0.98	1.29
[O III](λ4959 + λ5007)/[OII](λ3726 + λ3729)	39.4	39.5	16.3	16.6
[O II]λ3729/λ3726	0.58	0.60	0.54	0.52
C III]λ1909/λ1907	0.79	0.79		0.77
[O III](λ4959 + λ5007)/λ4363	87.6	76.0	81.3	84.6
He Iλ4471	3.77	4.04	3.75	3.87
He Iλ5876	11.1	11.0	10.4	10.4
He IIλ1640	199.	201.	284.	288.
He IIλ4686	28.6	28.3	40.7	40.6
C IIλ1335	27.4	27.8		52.9
C IIλ4267	0.78	0.23		0.45
C III]$\lambda\lambda$1907, 1909	1107.	1130.	1643.	1610.
C IV$\lambda\lambda$1548, 1550	1205.	1593.	1610.	2077.
[N II]$\lambda\lambda$6548, 6584	11.1	11.0	30.2	30.0
[O II]$\lambda\lambda$3726, 3729	29.1	29.2	78.7	76.7
[O II]λ7325	4.92	3.05	5.91	8.37
[O III]$\lambda\lambda$4959, 5007	1147.	1153.	1284.	1273.
O III]λ1663	66.9	32.5	80.3	30.3
[Ne III]$\lambda\lambda$3868, 3967	94.0	94.3	105.	104.
[Ne IV]λ4725	0.25	0.20	0.44	0.22
[Ne V]λ3425	5.79	7.57	27.8	17.0
[S II]$\lambda\lambda$6716, 6731	3.77	2.73	7.70	7.71
[S III]λ6312	0.80	1.33		1.13
Nebular ionized mass $M_{\rm ion}$(H + He) ($M_\odot$)	0.180		0.194	
SMC H-burning central stars:				
Star mass M_c ($M_\odot$)	0.674		0.649	
Evolutionary age since $T_{\rm eff} = 10^4$ K (yr):	4000		5500	
Predicted $\log g$:	5.48		5.99	
LMC He-burning central stars:				
Star mass M_c ($M_\odot$)	0.695		0.675	
Evolutionary age since $T_{\rm eff} = 10^4$ K (yr):	2700		7800	
Predicted $\log g$:	5.50		6.01	

ates from a radiative recombination process and thus its emissivity is nearly independent of density and has only a weak dependence on temperature. These fundamental properties of photoionized gaseous nebulae allow one to convert an observed nebular Hβ surface brightness distribution into a corresponding density distribution, provided the nebular geometry is known.

A formalism to convert the observed Hβ surface brightness distribution to a density distribution under the assumption of spherical symmetry is given by Harrington & Feibelman (1983). They use a density distribution of the form

$$N_{\rm H}(\rho) = N_0 \sum_{k=0}^{K} \sum_{n=0}^{N} a_{k,n} (\rho/H_k)^{2n} \exp[-(\rho/H_k)^2], \qquad (1)$$

where ρ is the radial distance from centre, H_k and N_0 are scaling factors for radius and density, $a_{k,n}$ are dimensionless

constants, and K and N are integers. Assuming uniform electron temperature and that hydrogen is fully ionized everywhere, it can be shown that the projected surface brightness distribution that results from such a density distribution is a function of the impact parameter of the line of sight, r, of similar form

$$I(r)=\sum_{k=0}^{K}\sum_{n=0}^{N} b_{k,n}(r/H_k)^{2n}\exp[-(r/H_k)^2], \quad (2)$$

where $b_{k,n}$ are functions of $a_{k,n}$ and H_k. A remarkable property of the brightness distribution of this form is that convolution of it with a Gaussian beam,

$$G(x,y)=\frac{1}{\pi s^2}\exp\left(-\frac{x^2+y^2}{s^2}\right),$$

results in another expression of exactly the same form; only the constants are changed. That is, the broadened brightness distribution is given by

$$S(r)=\sum_{k=0}^{K}\sum_{n=0}^{N} c_{k,n}(r/Q_k)^{2n}\exp[-(r/Q_k)^2], \quad (3)$$

where $Q_k^2=H_k^2+s^2$, and $c_{k,n}$ are functions of $b_{k,n}$ and H_k/Q_k. The angular resolution of the *HST* is not limited by atmospheric broadening (seeing); however, the small angular sizes of the Magellanic Cloud PN mean that the finite angular resolution of the *HST* needs to be taken into account when comparing the observed Hβ surface distribution with the predictions of modelling calculations. For a telescope of diameter D, the angular resolution is limited by the diffraction limit given by $\Delta\theta=1.22\lambda/D$, where λ is the observing wavelength. For the *HST*, $\Delta\theta=0.05$ arcsec at the wavelength of Hβ. In the analysis below we have assumed an *HST* angular resolution of 0.05 arcsec for both Hβ and [O III] λ5007 images, and have convolved the theoretical brightness distributions with a Gaussian of 0.05 arcsec FWHM (or in terms of Harrington & Feibelman's parameter $s=0.03$ arcsec) before comparing them to the observations. In practice, the density distribution is derived by varying $a_{k,n}$ until the resultant $S(r)$ matches the observations. Note that N_0 is not a free parameter, but is constrained by the absolute Hβ flux.

Strictly speaking, the Harrington & Feibelman formalism is valid only if the nebula is optically thin, i.e. if the nebula is fully ionized everywhere. As we will see below, SMC N 2 is found to be fully ionized. For this nebula, the density distribution deduced in the above manner reproduces correctly the Hβ brightness distribution after the ionizing radiation field had been adjusted to reproduce the ionization structure and Hβ luminosity (see below) and no iteration was required. This is not the case for SMC N 5, which is found to be optically thick and radiation-bounded, as indicated by its quite strong [O II] $\lambda\lambda$3726, 3729 line emission, in spite of its stronger He II λ4686 emission as compared to SMC N 2. For SMC N 5, several iterations were required to match both the ionization structure and the Hβ brightness distribution.

Finally, photoionization models based on density distributions derived as described above generally give an average density too low to reproduce density-sensitive line ratios such as [O II] $I(\lambda3729)/I(\lambda3726)$ and C III] $I(\lambda1909)/I(\lambda1907)$, indicating the presence of density fluctuations. A standard way to overcome this difficulty is to introduce the so-called filling factor, ε, such that within any small region a fraction ε of the volume is filled with material of density $N_{\rm H}(\rho)$, while the complementary fraction $(1-\varepsilon)$ is empty. For SMC N 2 and SMC N 5 our best-fitting models give $\varepsilon=0.405$ and 0.700, respectively.

The density distributions for SMC N 2 and SMC N 5, which reproduced the correct ionization structure, Hβ brightness distribution, absolute Hβ flux and observed density-sensitive line ratios, are shown in Figs 3(a) and (b). As in the case of IC 3568 studied by Harrington & Feibelman (1983), both SMC N 2 and SMC N 5 show a sharp drop in brightness near the nebular centre (Fig. 2) and it is thus

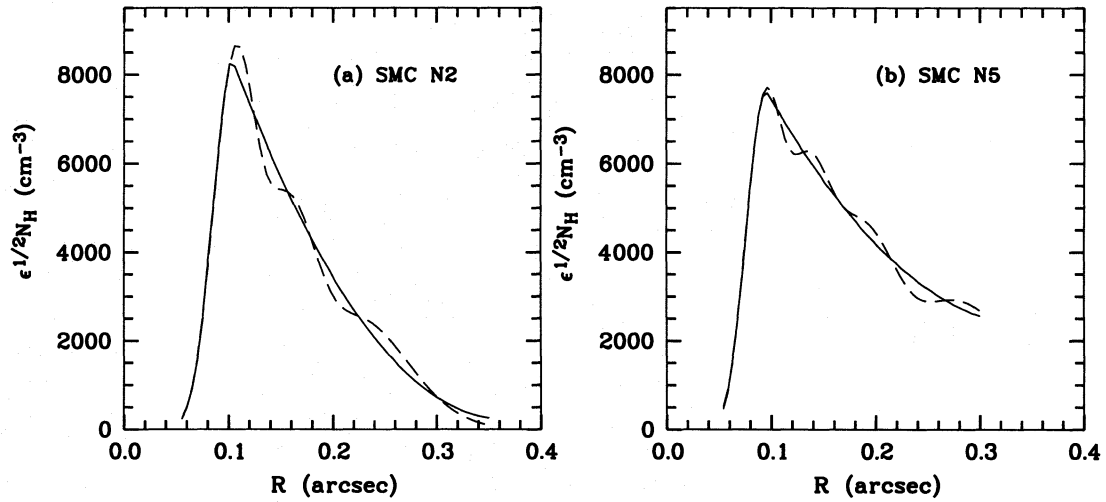

Figure 3. Density distributions of (a) SMC N 2 and (b) SMC N 5 derived from *HST* FOC Hβ images using the Harrington & Feibelman formalism (dashed lines). ε is the filling factor and equals 0.405 and 0.700 for SMC N 2 and SMC N 5, respectively. The density distributions adopted in our final photoionization models for these two nebulae are given by solid lines which are two-part polynomial fits to the dashed lines. See text for more details.

necessary to use a density distribution with a large value of N in equation (1). Here we have adopted $N=12$ for both nebulae. Large values of N result in very sharp, thin shells. To reproduce the extended, slowly decreasing brightness outside the peak emission, several shells are added together. In our case, $K=3$ and 4 have been used for SMC N 2 and SMC N 5, respectively.

Fig. 3 shows that SMC N 2 and SMC N 5 have very similar density structures, i.e. a central cavity surrounded by a thick shell whose density decreases slowly as radius increases. We have used low-order polynomials to fit the relatively rough density distributions derived using equation (1). Indeed, we find that a second-order polynomial is sufficient to describe the density variation in the thick shell for both nebulae. Such fits are shown in Fig. 3 and are adopted as the density distributions in our final models.

3.2 Photoionization models

Once the density distribution is established from the Hβ brightness distribution, using either the formalism of Harrington & Feibelman (1983) in the case of SMC N 2, or just based on test-and-try as in the case of SMC N 5, photoionization models which reproduce the correct ionization structure, i.e. models which match the observed line ratios such as $I(\lambda4686)/I(\lambda5876)$ and $I(\lambda4959+\lambda5007)/I(\lambda3726+\lambda3729)$, and the absolute H$\beta$ flux, are constructed using the code written originally by Dr J. P. Harrington and later revised and updated by Dr R. E. S. Clegg (see Harrington et al. 1982 and Clegg et al. 1987 for a description). The free parameters include the effective temperature $T_{\rm eff}$, luminosity L_* and surface gravity log g of the exciting star. The filling factor is also treated as a free parameter such that both the absolute Hβ flux and density-sensitive line ratios such as C III] $I(\lambda1909)/I(\lambda1907)$ and [O II] $I(\lambda3729)/I(\lambda3726)$ are matched. The Auer & Mihalas (1972) hydrogen and helium blanketed NLTE model atmospheres published by Clegg & Middlemass (1987) are adopted for the energy distribution of the exciting stars. Chemical abundances derived by Walton et al. (in preparation) based on a semi-empirical icf method were used as the first approximation. The Hβ surface brightness distributions predicted by the models were then convolved with a Gaussian of FWHM 0.05 arcsec and compared to those deduced from the *HST* images. This process was repeated until a model which matched all these constraints was reached. Finally, the chemical abundances were adjusted and the free parameters fine-tuned so that the absolute fluxes of well-measured lines such as He II $\lambda4686$, C III] $\lambda\lambda1907$, 1909, [N II] $\lambda6584$ and [O III] $\lambda5007$ were matched. The resultant abundances are in excellent agreement with those derived previously by Aller et al. (1987) for SMC N 2 and SMC N 5, and by Barlow et al. (1986) for SMC N 2.

The input parameters of the final models for SMC N 2 and SMC N 5 are listed in Table 1, where predictions from the models are compared to observed values. As can be seen in Table 1, excellent agreement is achieved between observations and model calculations for all important diagnostic line ratios as well as with the absolute fluxes of all important lines that are well measured. The only exception is the C IV $\lambda\lambda1548$, 1550 lines where, for both nebulae, the models give fluxes about 30 per cent higher than observed. Such a discrepancy is frequently encountered in nebular photoionization modelling calculations, and is generally attributed to the effect of dust absorption on these two resonance lines (e.g. Harrington et al. 1982). The effect is, however, much smaller than in Galactic PNe such as NGC 7662, modelled by Harrington et al., and NGC 3918, modelled by Clegg et al. (1987), indicating much smaller dust optical depths in these two SMC PNe. Our models also predict much smaller O III] $\lambda1663$ line fluxes, probably because of the observational errors involved in measuring this weak line, which consists of two components spanning a wavelength range of several ångströms. Finally, for SMC N 2, the model predicts a slightly low [O III] $I(\lambda4959+\lambda5007)/I(\lambda4363)$ line ratio, implying a higher average electron temperature, 14 300 K, as compared to the 13 400 K implied by the observed ratio. This may partly be due to observational error in the intensity of the relatively weak auroral line $\lambda4363$. The intensities of the [O III] optical lines of SMC N 2 adopted here are based on observations by Aller et al. (1981). For comparison, measurements presented by Meatheringham & Dopita (1991) give $I(\lambda4959+\lambda5007)/I(\lambda4363)=59.1$, implying $T_e=16\,000$ K. A better measurement of the $\lambda4363$ line is thus required in order to clarify the situation.

A remarkable feature of our photoionization model for SMC N 2 is that it successfully reproduces the accurate density diagnostic ratios of C III] $I(\lambda1909)/I(\lambda1907)$ and [O II] $I(\lambda3729)/I(\lambda3726)$, even though the former indicates an electron density three times higher than does the latter (Section 2.2). This strongly supports the validity of the density structure we deduced for this nebula from its *HST* Hβ image.

The model monochromatic surface brightness distributions in the Hβ and [O III] $\lambda5007$ lines, before and after convolution with a Gaussian of FWHM 0.05 arcsec, are plotted in Fig. 2 for SMC N 2 and SMC N 5. In both cases, although the broadened theoretical Hβ brightness distributions closely match what is observed, the models fail to reproduce the $\lambda5007$ brightness distributions: the observed $\lambda5007$ brightness outside the peak emission decreases much more slowly than predicted. The origin of this discrepancy is not clear. One possibility is that the nebulae are not strictly spherically symmetric, as can be seen on the Hβ image of SMC N 2. Thus our spherically symmetric models are only one-dimensional approximations to the real, three-dimensional objects. Even so, it is still hard to understand why this is not revealed in the Hβ images. Another possibility is that the model atmospheres adopted here are not good enough in giving the correct fluxes in the O^0 and O^+ ionizing continua. Clegg & Middlemass (1987) argued that the 'mean light-ion' of Mihalas (1972) produces 'artificial' absorption edges which do not occur in actual stellar flux distributions and were hence excluded from their calculations. The opacity of metal ions in photosphere or in stellar winds could, however, have effects on the emerging stellar ionizing flux that are worth further investigation. The modelling of additional nebulae of different properties may help to clarify the situation.

The variation of electron temperature, electron density, and the ionization structure of H, He, C, N and O, as functions of radius, in SMC N 2 and SMC N 5, that are predicted by our nebular models are shown in Figs 4 and 5. SMC N 2 is found to be completely ionized. H is still 95 per cent ionized at the outer boundary of our nebular model for SMC N 2, at

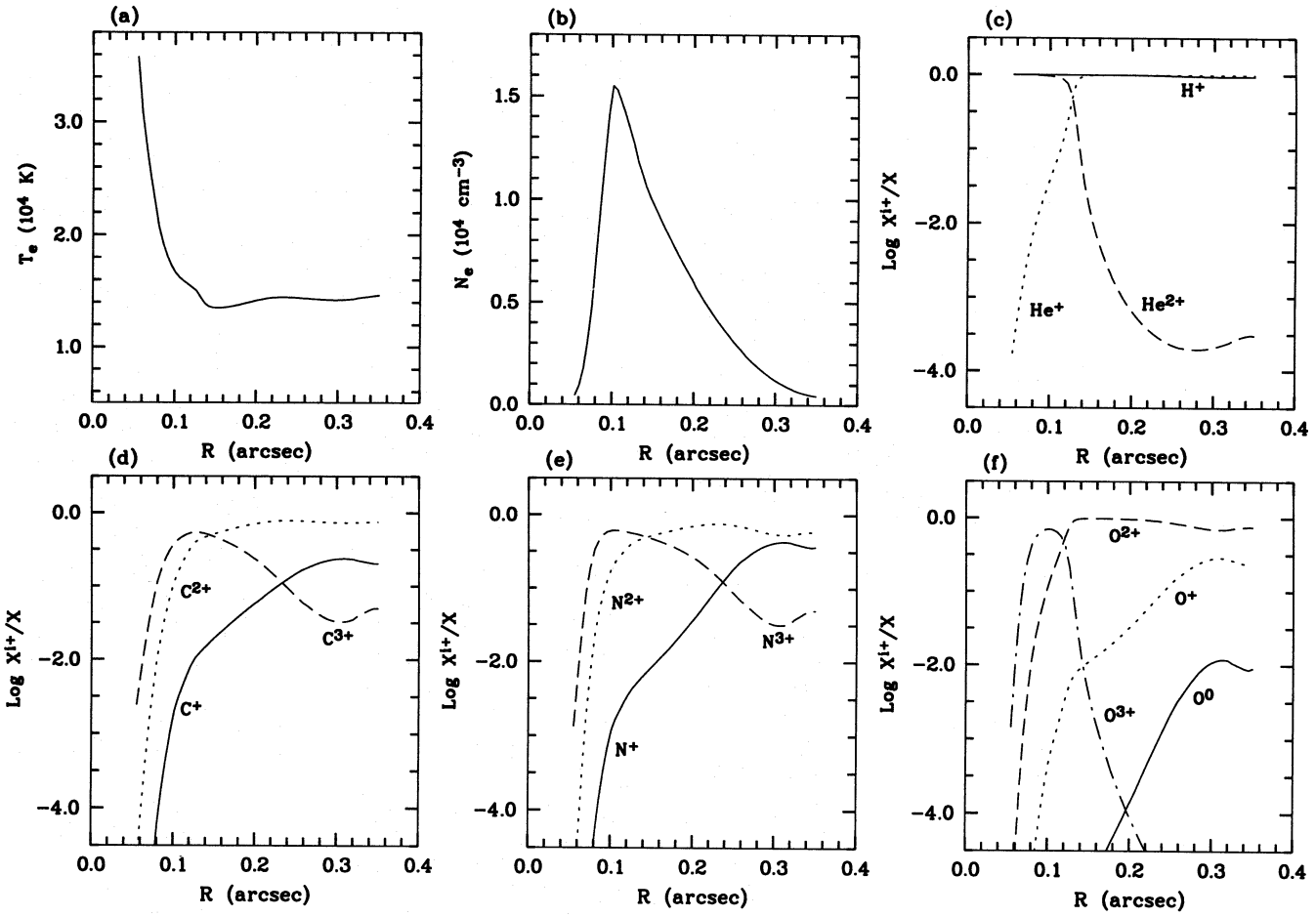

Figure 4. The variation of (a) electron temperature, (b) electron density and ionization fractions X^{i+}/X for (c) hydrogen and helium (d) carbon, (e) nitrogen and (f) oxygen, as a function of nebular radius as predicted by our photoionization model for SMC N 2.

a radius of 0.35 arcsec (0.102 pc), where the Hβ surface brightness has dropped to about 0.05 per cent of its peak value, which occurs at a radius of 0.096 arcsec. The optical depth at the H ionizing threshold at this outer radius is, however, quite significant, $\tau(H^0) = 54$, indicating that most of the ionizing photons from the central star should have been absorbed within the nebula. Unlike SMC N 2, however, SMC N 5 is radiation-bounded: H^+/H drops below 0.5 at a radius of 0.237 arcsec (0.0692 pc). At the outer boundary of our model for SMC N 5, at $r = 0.30$ arcsec, $H^+/H \approx 7 \times 10^{-4}$ and $\tau(H\,I) \approx 1300$.

Our photoionization models predict V magnitudes of 20.9 and 21.6, respectively, for the central stars of SMC N 2 and SMC N 5. For SMC N 2, the Hβ surface brightness near the nebular centre is about 1.2×10^{-12} erg cm^{-2} s^{-1} arcsec^{-2}, or for a pixel size of 0.0224 arcsec, 6.0×10^{-16} erg cm^{-2} s^{-1} pixel^{-1}. The predicted continuum emission from its central star at the corresponding wavelength is 9.9×10^{-16} erg cm^{-2} s^{-1}, assuming an effective bandwidth of 36.7 Å for the Hβ filter (Section 2.1). Thus, even if all the emission from the central star of SMC N 2 is caught by a single pixel on the Hβ image, it would still be very difficult to pick it out from the surrounding nebular Hβ emission background. The optical emission from the central star of SMC N 5 is even fainter, and a similar conclusion can be drawn. These results are consistent with the fact that no central stars were detected on our *HST* Hβ and [O III] λ5007 images of these two nebulae (Section 2.1). The central stars would be much easier to detect by imaging through a continuum filter (e.g. at 4200 Å). Meatheringham & Dopita (1991) report the detection of stellar emission from SMC N 5 from their optical spectrophotometry. They derived H and He$^+$ Zanstra temperatures of 126 000 and 155 000 K, respectively. Their detection is, however, doubtful considering the faintness of stellar emission as compared to the (total) nebular continuum emission. For example, at the wavelength of 4200 Å, the expected stellar flux is only 6 per cent of that from the nebular continuum. Note that from photoionization modelling calculations, Dopita & Meatheringham (1991) derived $T_{\rm eff} = 147\,000$ K and $L_* = 2780\ L_\odot$ for the exciting star of SMC N 5, which predicts even fainter stellar optical emission. The best opportunity for detecting these hot stars is, however, in the UV wavelength region. For this purpose we have investigated the *IUE* SWP spectra available for SMC N 2 and SMC N 5, which are plotted in Fig. 6. Unfortunately, after the contribution from nebular continuum emission has been subtracted, no stellar continuum can be detected above the noise level for both objects. The stellar and nebular continuum fluxes predicted by our models are shown in Fig. 6. For SMC N 5, the weakly detected con-

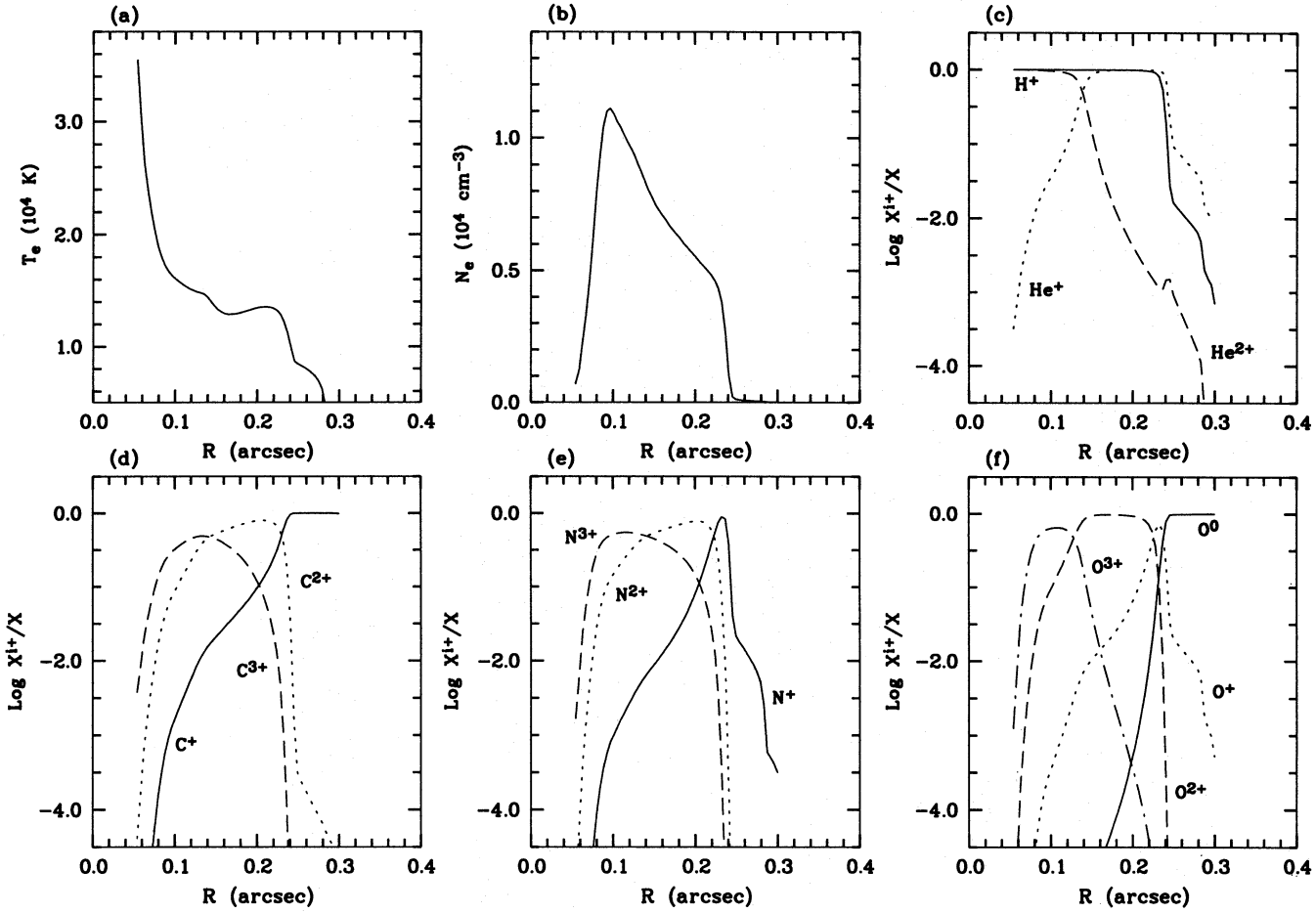

Figure 5. Same as Fig. 4, but for SMC N 5.

tinuum is dominated by the contribution from the nebular continuum. For SMC N 2, although our model predicts that the stellar continuum becomes dominant for $\lambda \leq 1600$ Å, the S/N ratio of the spectrum does not warrant a reliable determination of the stellar continuum. The predicted total continuum flux (stellar plus nebular) is, however, consistent with the observations.

A detailed photoionization model of SMC N 2 was presented previously by Barlow et al. (1986). From their speckle interferometric data they deduced a double-ring structure which is, however, inconsistent with the new *HST* image. As described in Section 1, the interpretation of speckle interferometric data is model-dependent. For example, Standley (1986) obtained a good fit to the same data set used by Barlow et al. (1986) with a single-ring model. On the other hand, parameters such as $T_{\rm eff}$ and log g derived by Barlow et al. for SMC N 2 are in close agreement with those derived here, indicating that the overall nebular excitation structure is not very sensitive to the actual density structure. This point is also supported by our test modelling calculations. However, the stellar luminosity deduced by Barlow et al. for this object, 4340 $L_\odot$ for the distance of 57.5 kpc adopted by them for the SMC, corresponding to 4767 $L_\odot$ for the distance of 60.3 kpc to the SMC adopted here, is much lower than the value of 8430 $L_\odot$ found here. This discrepancy may arise from the incorrect density distribution that they adopted.

We have also constructed test models treating the [O III] images as if they were Hβ images. For both nebulae, although stellar effective temperatures and surface gravities similar to those derived using the correct Hβ images were found, when using the [O III] images much higher stellar luminosities were required to reproduce the observed spectra, which violated the constraints on the stellar continua provided by the *IUE* observations. This stresses the importance of Hβ images in deriving correct stellar luminosities.

4 DISCUSSION

4.1 Nebular masses

The nebular *ionized* masses (H + He) of SMC N 2 and SMC N 5, integrated over the whole volume, are listed at the end of Table 1 and are 0.180 and 0.194 $M_\odot$, respectively. Since SMC N 2 is fully ionized, 0.180 $M_\odot$ should be the total mass of the gaseous shell. SMC N 5 is, however, radiation-bounded; hence the ionized mass found here is a lower limit to the total nebular (ionized plus neutral) mass. It is impossible to derive the total nebular mass for this object without knowing something about the mass in neutral form. Integra-

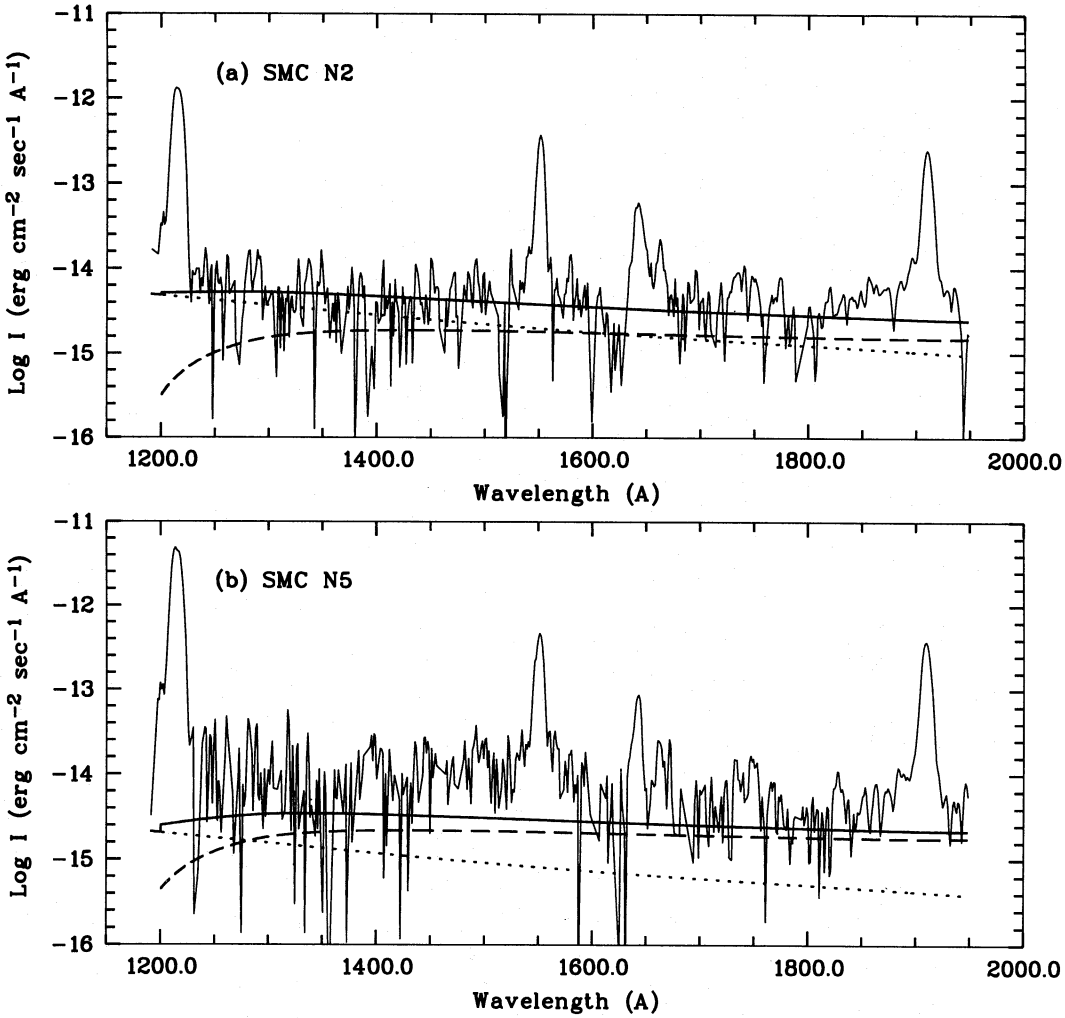

Figure 6. The dereddened *IUE* spectra of (a) SMC N 2 (formed by merging the spectra from SWP 14078, 20454 and 20527) and (b) SMC N 5 (formed by merging the spectra from SWP 14076, 14077 and 20453). The dotted and dashed lines are the predicted contributions from the central star and nebular continuum emission, and the solid lines are the sum of these. Note that the flux is plotted on a logarithmic scale, where all pixels with negative values have been discarded.

tion of the density distribution adopted here, shown in Fig. 3, to infinite radius will simply give an infinite value. Obviously, this density distribution should be cut off beyond a certain radius.

As described in Section 1, accurate nebular masses for PNe are important for a number of purposes. In order to derive nebular masses, we generally need to know nebular sizes or, preferably, nebular density distributions. Such information is, however, difficult and time-consuming to obtain for PNe such as those in the Magellanic Clouds, due to their very small angular sizes. A method to deduce nebular ionized masses without knowing the nebular sizes was proposed by Barlow (1987) who showed that the ionized mass of a PN can be derived from its absolute Hβ flux, provided its mean electron density is known, i.e.

$$M_{\rm ion}=\frac{8.12\times10^{11}I(\mathrm{H}\beta)\,t^{0.913}(1+4y)\,D^2(\mathrm{kpc})}{\langle N_{\rm e}\rangle}\,\mathrm{M}_\odot, \qquad (4)$$

where $t=T_{\rm e}/10^4$ K, y is the He abundance by number, D is the distance to the nebula and $\langle N_{\rm e}\rangle$ is the mean electron density derived from a density-sensitive forbidden line ratio. The key point of this method is to find an observable density-sensitive ratio of two emission lines whose emissivities trace closely the nebular overall ionized mass distribution and from which an $\langle N_{\rm e}\rangle$ characteristic of the whole nebula can be determined. Barlow (1987) argued that for optically thin PNe, most of the O^+ giving rise to the emission of the [O II] $\lambda\lambda$3726, 3729 doublet (whose ratio is a sensitive probe of electron density) arises from recombination of electrons with O^{2+} ions, which, as a dominant ion, should trace the ionized gas well. Thus, for optically thin nebulae, the electron density deduced from the [O II] doublet ratio should give a good approximation to $\langle N_{\rm e}\rangle$, provided that fluxes integrated over the whole nebula are used for both lines. The photoionization models presented here can be used to test this method. Using the C III] $I(\lambda1909)/I(\lambda1907)$ and [O II] $I(\lambda3729)/I(\lambda3726)$ line ratios given by our photoionization model for SMC N 2, we find $\langle N_{\rm e}(\mathrm{C\,III])}\rangle=7770$ cm^{-3} and $\langle N_{\rm e}([\mathrm{O\,II}])\rangle=2730$ cm^{-3}. Substitution of these two densities into equation (4) yields $M_{\rm ion}$ equal to 0.156 and 0.444 $\mathrm{M}_\odot$, respectively. Similarly, for SMC N 5, $\langle N_{\rm e}(\mathrm{C\,III])}\rangle=6670$

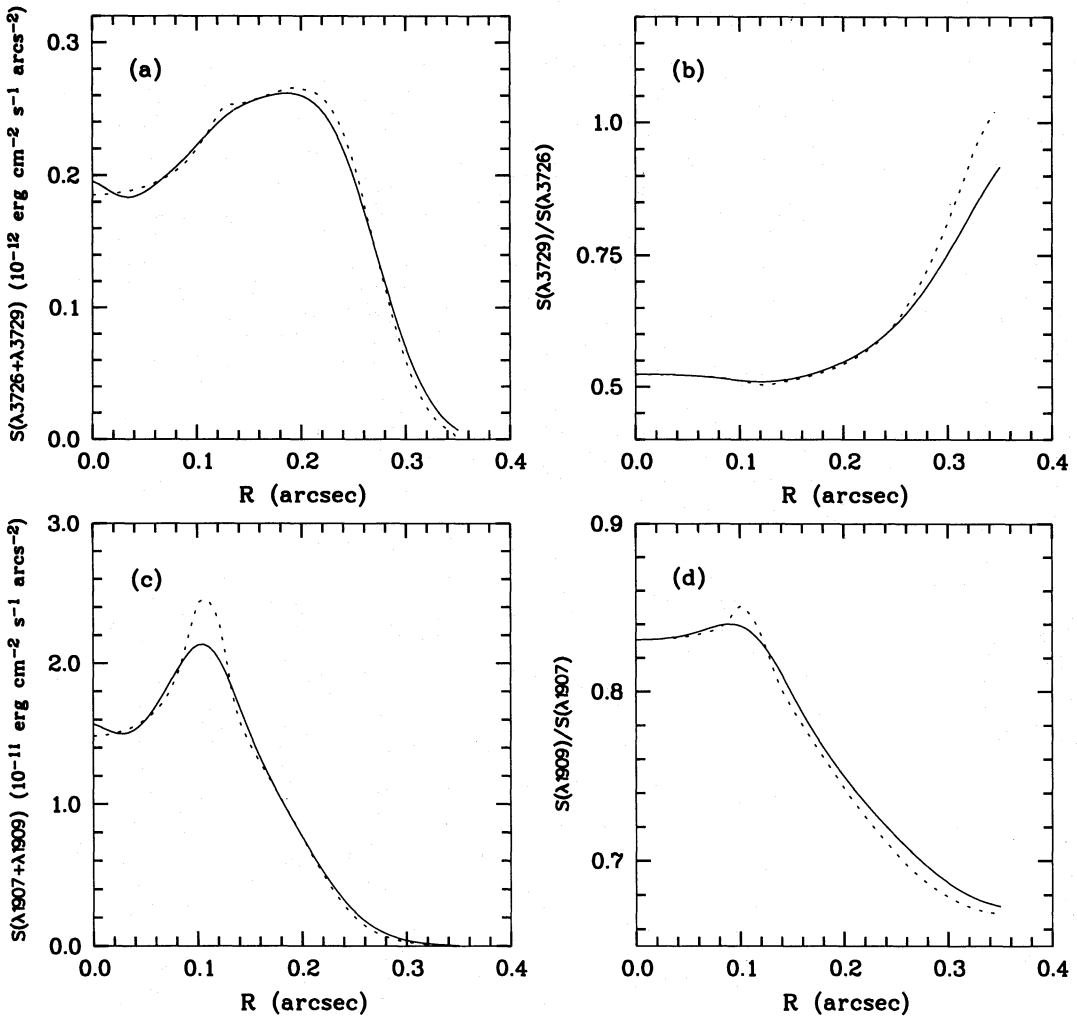

Figure 7. Diagrams showing the radial variations of the surface brightness of (a) the [O II] λλ3726, 3729 lines, and (b) their ratio, (c) the surface brightness of the C III] λλ1907, 1909 lines, and (d) their ratio, for SMC N 2 as derived from our photoionization model for this nebula. The dotted and solid lines are, respectively, the intrinsic surface brightness distributions predicted by the model, and the same distributions after convolution with a Gaussian of FWHM of 0.05 arcsec.

cm^{-3} and $\langle N_e([O\,II])\rangle = 4370\ cm^{-3}$, yielding ionized nebular masses of 0.197 and 0.300 $M_\odot$, respectively. These results may be compared to the actual nebular ionized masses of 0.180 and 0.194 $M_\odot$ listed in Table 1 for SMC N 2 and SMC N 5. Obviously, even for SMC N 2, which is optically thin, the M_{ion} derived from the mean [O II] density overestimates the actual value. On the other hand, for both objects the nebular mass M_{ion} derived from the mean C III] density provides a good approximation to the real value. This result can be understood by comparing the nebular density distributions shown in Fig. 3 with the surface brightness distributions of the C III] and [O II] lines presented in Figs 7 and 8. Even for SMC N 2, most of the [O II] emission comes from the outer part of the nebula, where the density has dropped significantly. In contrast, the C III] lines trace much better the overall distribution of nebular mass, owing to the higher ionization potential of C^+ as compared with that of O^0.

4.2 Central star masses

Once the effective temperature and luminosity have been determined, the mass of the central star can be derived by interpolating between theoretical evolutionary tracks. The result depends on whether the star is assumed to be burning hydrogen or helium in a thin shell above its CO core, which in turn depends on the phase of the thermal pulse cycle at which the departure from the AGB occurs. In the HR diagram in Fig. 9, the luminosities of the central stars of SMC N 2 and SMC N 5 are plotted against their effective temperatures. Also shown are H- and He-burning evolutionary tracks calculated by Vassiliadis & Wood (1994) for progenitor stars with heavy-element abundances corresponding to the mean metal abundances of the LMC ($Z = 0.008$) and SMC ($Z = 0.004$). The stellar masses derived by interpolating between the SMC H-burning tracks and the LMC He-burning tracks (for progenitor stars with an SMC mean metal composition, only one He-burning track, for a core mass of 0.558 $M_\odot$, was calculated by Vassiliadis & Wood 1994), and the corresponding evolutionary ages since the stars first reached an effective temperature of 10 000 K, are listed at the end of Table 1. (The results listed for SMC N 2 as a He-burner were derived by extrapolating the two LMC He-burning tracks for masses of 0.669 and 0.679 $M_\odot$, the largest core masses calculated by Vassiliadis &

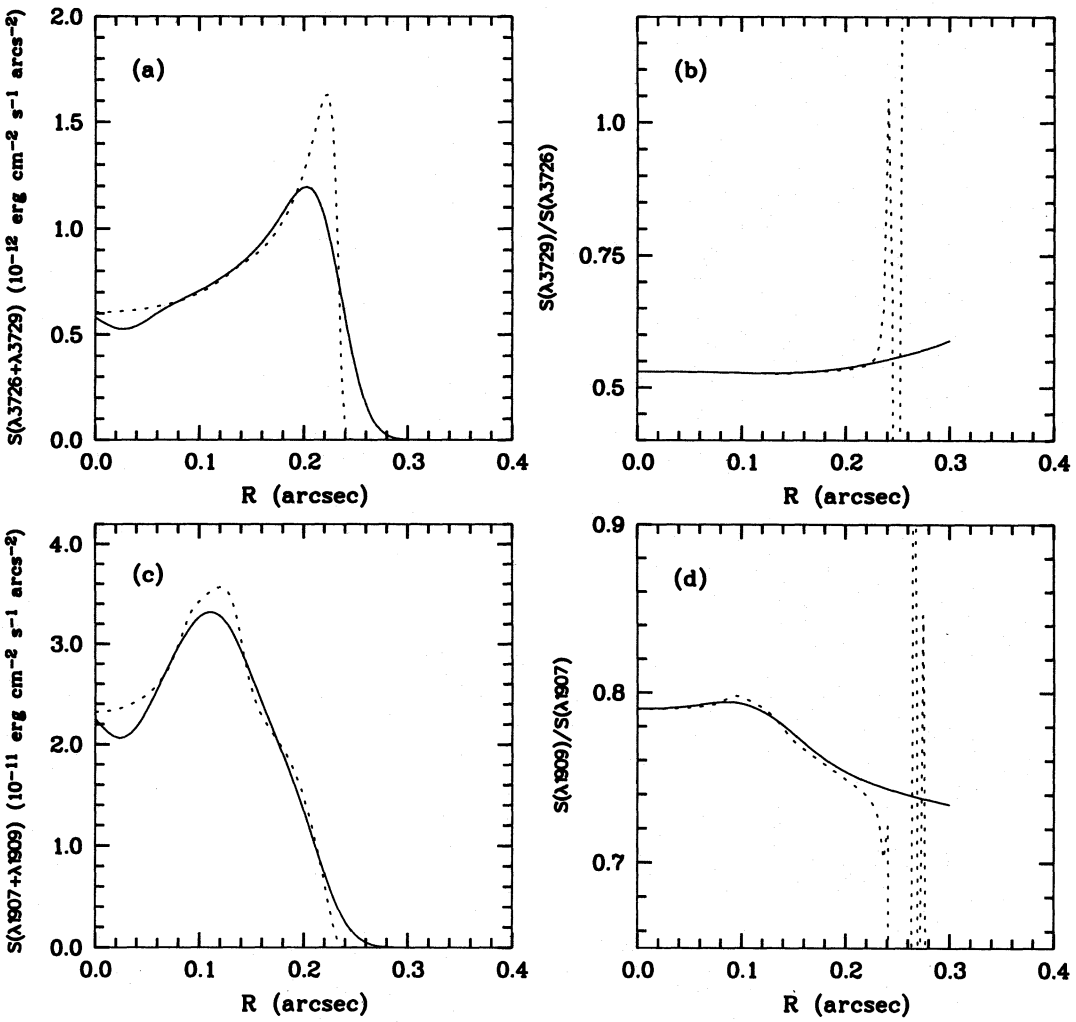

Figure 8. Same as Fig. 7, but for SMC N 5. The sharp variations seen in the dotted lines in (b) and (d) near the nebular edge are artefacts produced by numerical rounding errors. The nebula becomes neutral at a radius of approximately 0.24 arcsec (cf. Fig. 5), and so the [O II] and C III] line fluxes beyond this point are essentially zero.

Wood for He-burners.) From the radius (which can be calculated from the effective temperature and luminosity) and the mass of the central star, the stellar surface gravity can be derived. The results are also listed in Table 1, and are in close agreement with the values used to construct the nebular photoionization models.

As described in Section 3, although accurate determination of stellar luminosities by modelling calculations requires realistic nebular density distributions such as those derived from the Hβ surface brightness distributions, stellar effective temperatures $T_{\rm eff}$ and surface gravities log g deduced from such calculations are not very sensitive to the actual density distributions. Reasonably accurate values of $T_{\rm eff}$ and log g can be derived even using density distributions derived from images taken in the light of the [O III] λ5007 line, treated as if they were taken in Hβ. It is thus interesting to see whether reliable values of the stellar core mass can be derived from $T_{\rm eff}$ and log g alone with the help of theoretical evolutionary tracks, without resort to stellar luminosity. Such a technique to derive $M_{\rm c}$ from $T_{\rm eff}$ and log g has been previously employed (e.g. Méndez et al. 1988; Méndez 1991) to study Galactic PNe for which distances and therefore luminosities are difficult to obtain, with the values of $T_{\rm eff}$ and log g derived by fitting high-spectral-resolution profiles of stellar H and He absorption lines with theoretical line profiles obtained from non-LTE model atmosphere calculations. For this purpose, we have rederived the stellar core masses for SMC N 2 and SMC N 5 by interpolating their $T_{\rm eff}$ and log g values derived from our photoionization modelling calculations between the H- and He-burning tracks of Vassiliadis & Wood (1994). From H-burning evolutionary tracks of mean SMC metal abundance, we find $M_{\rm c}=0.680$ and 0.648 $M_\odot$ for SMC N 2 and SMC N 5, respectively, in excellent agreement with the values of 0.674 and 0.648 $M_\odot$ listed at the end of Table 1, derived from the $T_{\rm eff}$ and L_* obtained from our modelling calculations. The above values of $M_{\rm c}=0.680$ and 0.648 $M_\odot$, together with the corresponding values of $T_{\rm eff}$ and log g yield luminosities L_* of 9200 and 5720 $L_\odot$ for SMC N 2 and SMC N 5, respectively, consistent with the (more accurate) luminosities listed in Table 1, which were derived directly from our modelling calculations. Similarly, from the He-burning evolutionary tracks of mean LMC metal abundance,

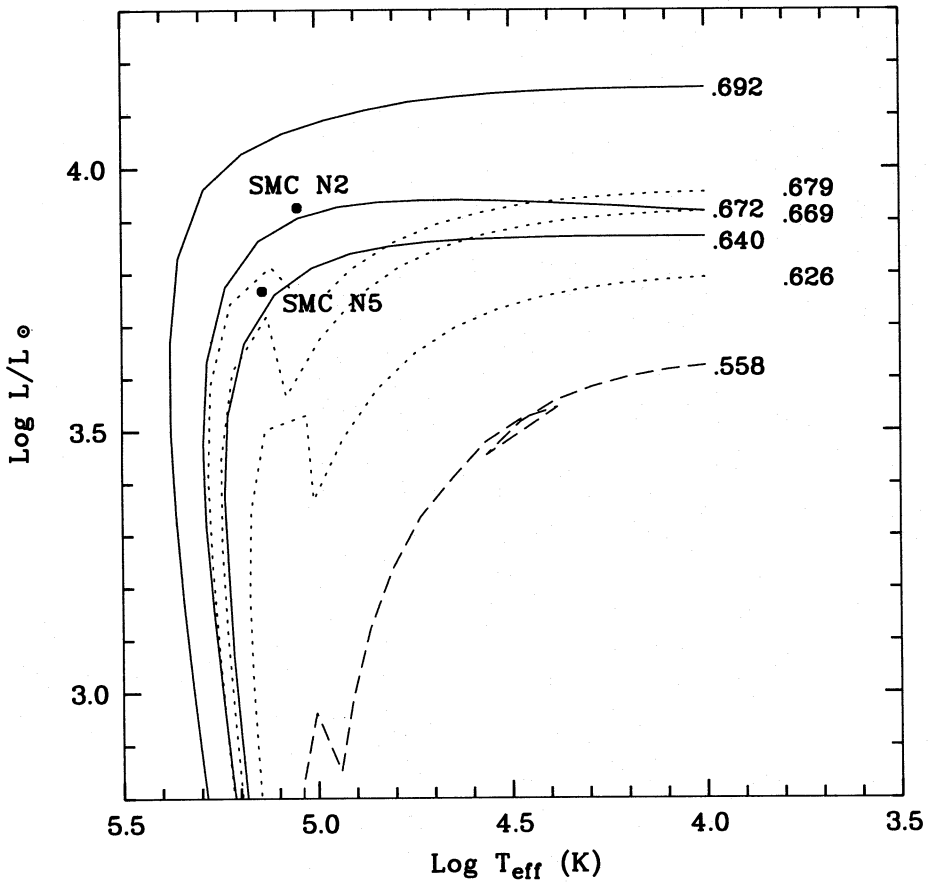

Figure 9. The HR diagram for SMC N 2 and SMC N 5, where stellar luminosity is plotted against effective temperature. The solid lines are H-burning evolutionary tracks for core masses of 0.640, 0.672 and 0.692 $M_\odot$, for progenitor stars of mean SMC heavy-element abundance ($Z=0.004$). Similarly, the dotted lines are He-burning tracks for core masses of 0.626, 0.669 and 0.679 $M_\odot$ of mean LMC abundance ($Z=0.008$), and the dashed line is a He-burning track for a core mass of 0.558 $M_\odot$ of mean SMC abundance. All the theoretical tracks are taken from Vassiliadis & Wood (1994).

we find $M_c=0.688$ and 0.677 $M_\odot$ for SMC N 2 and SMC N 5, respectively, in turn implying $L_*=9310$ and 5970 $L_\odot$, again in excellent agreement with those listed in Table 1. These calculations clearly show that reasonably accurate values of M_c (and thus L_*) can be derived with the aid of theoretical evolutionary tracks, provided that reliable values of $T_{\rm eff}$ and $\log g$ can be determined, either by photoionization modelling as used in this study, or by stellar absorption-line profile fitting as employed by Méndez et al. (1988) and Méndez (1991).

The evolutionary ages given at the end of Table 1 can be compared to the expansion ages of the gaseous shells. The [O III] λ5007 line profiles of SMC N 2 and SMC N 5 have been measured by Dr J. Meaburn using the University of Manchester Echelle Spectrometer (Meaburn et al. 1984) on the AAT at a resolution of 12.9 km s^{-1}. The result for SMC N 2 has been presented by Barlow et al. (1986). They gave an expansion velocity of 17 km s^{-1}. In their analysis, contributions from instrumental and thermal broadening to the observed linewidth were taken into account and they assumed that the nebular expansion velocity increases linearly with radius (Robinson, Reay & Atherton 1982). The expansion velocity thus obtained corresponds to that at the nebular peak emission. A similar analysis of the data for SMC N 5 shows that it has the same expansion velocity as SMC N 2, i.e. 17 km s^{-1}. In the light of Hβ, SMC N 2 and SMC N 5 have angular radii of 0.095 and 0.091 arcsec, respectively, at their peak surface brightness (Fig. 2). At the distance of 60.3 kpc adopted here for the SMC, the corresponding linear sizes of 0.028 and 0.026 pc yield expansion ages of 1600 and 1530 yr for SMC N 2 and SMC N 5, respectively. For SMC N 2, as already noted by Blades et al. (1992), the expansion age thus derived is too short as compared to the evolutionary age if the central star is on a H-burning evolutionary track, but is more easily reconciled if the star is on a He-burning track. For SMC N 5, however, both H-burning and He-burning assumptions give similar evolutionary ages, between 5500 and 7800 yr, much longer than the expansion age. Even if we assume that the nebular expansion velocity increases linearly with time from a starting value of 10 km s^{-1}, the expansion age increases by only about 30 per cent, still significantly lower than the evolutionary age. On the other hand, it is possible that the assumption that the expansion velocity increases linearly with radius is valid only for optically thin objects and not for SMC N 5, which is optically thick. For SMC N 5 the nebula extends beyond the ionization front boundary. Accordingly, the assumption that the expansion velocity of 17 km s^{-1} derived

above corresponds to expansion at the peak density may not be right, and the expansion age of SMC N 5 could be higher than the 1530 yr given above.

The above comparisons between the nebular expansion and evolutionary ages are based on an extremely simplified evolutionary scenario for PNe as uniform expanding shells. However, recent radiation-gasdynamics modelling of the evolution of PNe shows the importance of the evolution of the central star and its fast stellar wind on the nebular morphology and kinematics. For example, Mellema (1994) finds that the ionization of a nebula by its central star can lead to a stalling of the expansion of the nebula, giving an expansion age apparently lower than the corresponding evolutionary age [but see also Marten, Geşicki & Szczerba (1993) who find exactly the opposite result from independent numerical studies]. Our results on the expansion and evolution ages for SMC N 2 and SMC N 5 are consistent with the stalled expansion calculations of Mellema (1994). It should be noted, however, that the evolutionary ages quoted above, from Vassiliadis & Wood (1994), refer to the time since the central star had $T_{\rm eff} = 10^4$ K. Given that calculated time-scales for evolution from the AGB (which should correspond to the zero-point for the nebular expansion) to $T_{\rm eff} = 10^4$ K are very sensitive to the assumptions of the evolutionary models (Schönberner 1990; Vassiliadis & Wood 1994), it appears that comparisons between nebular expansion ages and central star evolutionary ages may not be very profitable at present.

4.3 Abundances

The chemical abundances derived from our modelling calculations for SMC N 2 and SMC N 5 are compared in Table 2 to values published previously by other workers (Barlow et al. 1986; Aller et al. 1987; Dopita & Meatheringham 1991; Walton et al. 1991 and in preparation). All the abundances listed in Table 2 are derived from photoionization modelling calculations, except those from Walton et al. where a semi-empirical icf method has been used. For C, O and Ne, the abundances generally agree within 0.05 dex (12 per cent), except for oxygen, for which Dopita & Meatheringham derived an abundance which was 0.2 dex lower in the case of SMC N 2, and 0.1 dex lower in the case of SMC N 5. Our helium abundances are about 0.04 dex lower than those given by Aller et al. (1987) and Barlow et al. (1986), and are in better agreement with those of Walton et al. This is because in Walton et al. and in the current work the effect of collisional excitation of the helium triplet metastable ground level (2^3S) by electron impacts, which enhance the observed helium line intensities, has been accounted for. The agreement between the nitrogen and sulphur abundances is, however, less satisfactory, with discrepancies of as large as 0.3 dex. The large scatter in the derived N and S abundances is simply due to the fact that for both elements only lines from a single ionization stage have been measured, i.e. [N II] $\lambda\lambda$6548, 6584 and [S II] $\lambda\lambda$6716, 6731. (For SMC N 2, the intensity of the [S III] λ6312 line has also been measured, but with a large uncertainty due to its weakness. Because of its high excitation energy, the flux of this line is very sensitive to the electron temperature.) In both SMC N 2 and SMC N 5, most nitrogen and sulphur exists in ionization stages higher than N^+ and S^+, and so N and S abundances based only on the [N II] and [S II] lines depend critically on the ionization structures determined by the modelling calculations.

Table 2. Logarithmic elemental abundances for SMC N 2 and SMC N 5 on scale where log N(H) = 12.00.

	He	C	N	O	Ne	S	Ref.
SMC N 2	11.04	8.83	7.30	8.17	7.41	6.28	(1)
	11.05	8.74	7.50	8.16	7.38	6.26	(2)
	11.11	-	6.84	7.95	7.34	6.25	(3)
	10.98	8.84	7.42	8.22	7.36	-	(4)
	10.99	**8.71**	**7.25**	**8.16**	**7.34**	**6.57**	(5)
SMC N 5	11.09	8.90	7.17	8.27	7.74	6.71	(2)
	11.11	-	7.20	8.18	7.40	6.65	(3)
	11.01	8.95	7.49	8.30	7.44	-	(4)
	11.05	**8.99**	**7.33**	**8.31**	**7.49**	**6.50**	(5)

(1) Barlow et al. (1986); (2) Aller et al. (1987); (3) Dopita & Meatheringham (1991); (4) Walton et al. (1991, and in preparation); (5) this work.

5 SUMMARY

We have constructed fully self-consistent photoionization models for two SMC PNe, SMC N 2 and SMC N 5, based on realistic nebular radial density distributions derived from *HST* FOC Hβ images. The models successfully reproduce the observed Hβ surface brightness distributions and all the important line fluxes obtained from optical and UV spectrophotometry. The models, however, fail to reproduce the surface brightness distributions in the [O III] λ5007 line, which has also been imaged by the *HST*. This discrepancy could arise from the crudeness of the model atmospheres used in the current calculations. Our modelling calculations show that although reliable values of $T_{\rm eff}$ and log g can be obtained by making use of [O III] surface brightness distributions, accurate density distributions derived by imaging in the light of 'proper' lines such as Hβ are crucial for obtaining reliable stellar luminosities by matching the nebular emission properties. An alternative way to obtain the stellar luminosities, however, is to derive the stellar core mass $M_{\rm c}$ directly by interpolating between theoretical evolutionary tracks in the $T_{\rm eff}$–log g plane, using the values of $T_{\rm eff}$ and log g derived from photoionization modelling fits to the observed line ratios, which are less dependent on the actual nebular density distributions. The resultant value of $M_{\rm c}$, together with the derived $T_{\rm eff}$ and log g, can then be used to calculate the stellar luminosity. It is found that the stellar luminosities deduced in this manner agree reasonably well with those derived from photoionization modelling matches to the observed nebular Hβ surface brightness distributions and line fluxes. We have also shown that the correct nebular ionized mass can be deduced from the nebular Hβ flux, provided that the mean nebular density given by the C III] λ1909/λ1907 ratio is also known.

ACKNOWLEDGMENTS

JCB and SO acknowledge support from NASA through Contract NAG5-1773.

REFERENCES

Aller L. H., Keyes C. D., Ross J. E., O'Mara B. J., 1981, MNRAS, 194, 613
Aller L. H., Keyes C. D., Maran S. P., Gull T. R., Michalitsianos A. G., Stecher T. P., 1987, ApJ, 320, 159
Auer L. H., Mihalas D., 1972, ApJS, 24, 193
Barlow M. J., 1987, MNRAS, 227, 161
Barlow M. J., 1989, in Torres-Peimbert S., ed., Proc. IAU Symp. 131, Planetary Nabulae. Kluwer, Dordrecht, p. 319
Barlow M. J., Morgan B. L., Standley C., Vine H., 1986, MNRAS, 223, 151
Blades J. C. et al., 1992, ApJ, 398, L41
Burstein D., Heiles C., 1982, AJ, 87, 1165
Clegg R. E. S., Middlemass D., 1987, MNRAS, 228, 759
Clegg R. E. S., Harrington J. P., Barlow M. J., Walsh J. R., 1987, ApJ, 314, 551
Dopita M. A., 1993, in Weinberger R., Acker A., ed., Proc. IAU Symp. 155, Planetary Nebulae. Kluwer, Dordrecht, p. 433
Dopita M. A., Meatheringham S. J., 1991, ApJ, 367, 115
Dopita M. A., Ford H. C., Bohlin R., Evans I. N., Meatheringham S. J., 1993, ApJ, 418, 804
Dopita M. A. et al., 1994, ApJ, 426, 150
Gathier R., Pottasch S. R., Goss W. M., Van Gorkom J. H., 1983, A&A, 128, 325
Harrington J. P., Feibelman W. A., 1983, ApJ, 265, 258
Harrington J. P., Seaton M. J., Adam S., Lutz J. H., 1982, MNRAS, 199, 517
Howarth I. D., 1983, MNRAS, 203, 301
Hummer D. G., Storey P. J., 1987, MNRAS, 224, 801
Jacoby G. H., 1980, ApJS, 42, 1
Keenan F. P., Feibelman W. A., Berrington K. A., 1992, ApJ, 389, 443
Lucy L. B., 1974, AJ, 79, 745
Marten H., Geşicki K., Szczerba R., 1993, in Weinberger R., Acker A., eds, Proc. IAU Symp. 155, Planetary Nebulae. Kluwer, Dordrecht, p. 315
Meaburn J., Blundell B., Carling R., Gregory D. F., Keir D., Wynne C. G., 1984, MNRAS, 210, 463
Meatheringham S. J., Dopita M. A., 1991, ApJS, 76, 1085
Meatheringham S. J., Dopita M. A., Morgan D. H., 1988, ApJ, 329, 166
Mellema G., 1994, A&A, 290, 915
Méndez R. H., 1991, in Michaud G., Tutukov A., eds, Proc. IAU Symp. 145, Evolution of Stars: The Photospheric Abundance Connection. Kluwer, Dordrecht, p. 375
Méndez R. H., Kudritzki R. P., Herrero A., Husfeld D., Groth H. G., 1988, A&A, 190, 113
Mihalas D., 1972, NCAR Tech. Note, TN/STR-76
Monk D. J., Barlow M. J., Clegg R. E. S., 1988, MNRAS, 234, 583
Nussbaumer H., Schild H., 1979, A&A, 75, L17
Nussbaumer H., Storey P. J., 1981, A&A, 99, 177
Osmer P., 1976, ApJ, 203, 352
Prévot M. L., Lequeux J., Maurice E., Prévot L., Rocca-Volmerange B., 1984, A&A, 132, 389
Richardson W. H., 1972, J. Opt. Soc. Am., 62, 55
Robinson G. J., Reay N. K., Atherton P. D., 1982, MNRAS, 199, 649
Schönberner D., 1990, in Mennessier M. O., Omont A., eds, From Miras to Planetary Nebulae: Which Path for Stellar Evolution? Editions Frontières, Gif-sur-Yvette, p. 355
Standley C., 1986, PhD thesis, Univ. London
Vassiliadis E., Wood P. R., 1994, ApJS, 92, 125
Walton N. A., Barlow M. J., Clegg R. E. S., 1991, in Haynes R., Milne D., eds, Proc. IAU Symp. 148, The Magellanic Clouds. Kluwer, Dordrecht, p. 291
Webster B. L., 1983, PASP, 95, 610
Wood P. R., Bessell M. S., Dopita M. A., 1986, ApJ, 311, 632
Wood P. R., Meatheringham M. A., Dopita M. A., Morgan D. H., 1987, ApJ, 320, 178